Elasto-Plastic Stresses in a Functionally Graded Rotating Disk

Babak Haghpanah Jahromi

Hamid Nayeb-Hashemi

Ashkan Vaziri[1]

e-mail:vaziri@coe.neu.edu

Department of Mechanical and Industrial Engineering, Northeastern University, Boston, MA 02115

A numerical method based on the extension of the variable material property method was developed to obtain the elasto-plastic stress field in a functionally graded (FG) rotating disk. The method was applied to estimate the stress field in a metal–ceramic functionally graded solid disk. To establish the validity of the proposed method, results were compared with finite element results. Unlike uniform rotating disks, where yielding starts from the disk center, plasticity in FG disks can originate at any point. The effect of different metal–ceramic grading patterns as well as the relative elastic moduli and densities of the ceramic and metallic constituents on the developed stresses were studied. Reinforcement of a metal disk with ceramic particles, in both elastic and plastic regimes, can significantly influence the mechanical response of the disk such as the stress distribution and the critical angular velocities corresponding to the onset of plasticity in the disk and plastic disk. Disks with increasing ceramic content from inner to outer radius showed a more uniform von Mises stress distribution for a fixed value of total ceramic content. In contrast, disks with decreasing ceramic content from inner to outer radius had the lowest outer edge displacement for a fixed value of total ceramic content. [DOI: 10.1115/1.4006023]

Keywords: rotating disks, elasto-plastic analysis, functionally graded material, variable material properties method, analytical and numerical methods

1 Introduction

Rotating disks have broad applications in gas turbines, high speed gears, fly wheels, and compact discs. Optimizing the design of a rotating disk and also assessing the failure risk require understanding its behavior in the elasto-plastic regime. In this context, numerical and analytical investigations have been extensively used to predict the deformation, failure, and stress and strain fields in a uniform rotating disk under different loading conditions (e.g., see Refs. [1–7]). The stress field in a uniform rotating disk—under elastic or elasto-plastic loading condition—is not uniform and the maximum stress occurs at the center of the disk. The nonuniform distribution of stresses is a key barrier in designing rotating disks with enhanced performance (e.g., minimum weight design, maximum stored energy, minimum outer edge displacement, and uniform stress distribution). One avenue for addressing this challenge is to vary the thickness and/or density of the rotating disk along its radius to make the stress distribution near-uniform [8–13]. However, excessive manufacturing costs of such disks at high precision and restrictions due to the curved geometry generally make this solution infeasible. An alternative approach is to use materials with varying properties [14–16]. In this context, FG materials are promising candidates as they avoid the negative effects of abrupt changes in the material constituent due to their unique composition. Moreover, the manufacturing of FG disks with radially varying properties is technically possible by controlling the relative distribution of the disk material constituents (e.g., reinforcement particles and metal matrix) using techniques such as the centrifugal casting process [17–20].

The analysis of rotating objects (disk, shafts, beams, etc.) with varying material properties is generally challenging, since the interaction between different deformation modes could lead to a complex state of stress and deformation, including out of plane deformation, vibration, warping, and instability [21–26]. For a disk with material variation in the radial direction, the structure can be discretized to uniform rings of different radii with infinitesimal width. The elastic analysis for stress and deformation fields in a FG rotating disk with exponentially and parabolically varying elastic modulus in the radial direction is presented by Eraslan and Akis [27]. Similar semi-analytical and numerical studies have been carried out for FG elastic disks [28–31]. In this study, we provide an analytical method for estimating the elasto-plastic stresses in a rotating disk with varying elastic and plastic properties in the radial direction. The proposed method is an extension of the variable material properties (VMP) method [32,33], and is discussed in Sec. 2. In this method, the functionally graded material parameters are considered as field variables and the linear elastic solution of a boundary value problem is used to generate the inelastic solution in an iterative manner. The analysis method is applicable to both hollow and solid disks with different boundary conditions, multilayered rotating disks, disks with temperature gradients, and disks with varying thicknesses and material properties, as long as the problem has an axisymmetric condition. This method is generally very effective and the solution can be obtained after few iterations. The method also yields accurate solutions for the elasto-plastic stress distributions compared to other approaches such as the semi-analytical method presented by You and Zhang [1] for uniform elasto-plastic disks as explained in Sec. 3. In Sec. 4, we applied the method developed to analyze the elasto-plastic stresses in a FG rotating disk reinforced with ceramic particles. In this study, the constituent material of the rotating disk is considered to be a metal–ceramic composite with various ceramic volume fractions through the disk radius. A selected set of finite element calculations were done to establish the validity of the proposed method using the commercially available software ABAQUS. A parametric study was carried out to study the effect of variation of material properties on the distribution of

[1]Corresponding author.

Contributed by the Materials Division of ASME for publication in the JOURNAL OF ENGINEERING MATERIALS AND TECHNOLOGY. Manuscript received April 4, 2011; final manuscript received January 30, 2012; published online March 26, 2012. Assoc. Editor: Georges Cailletaud.

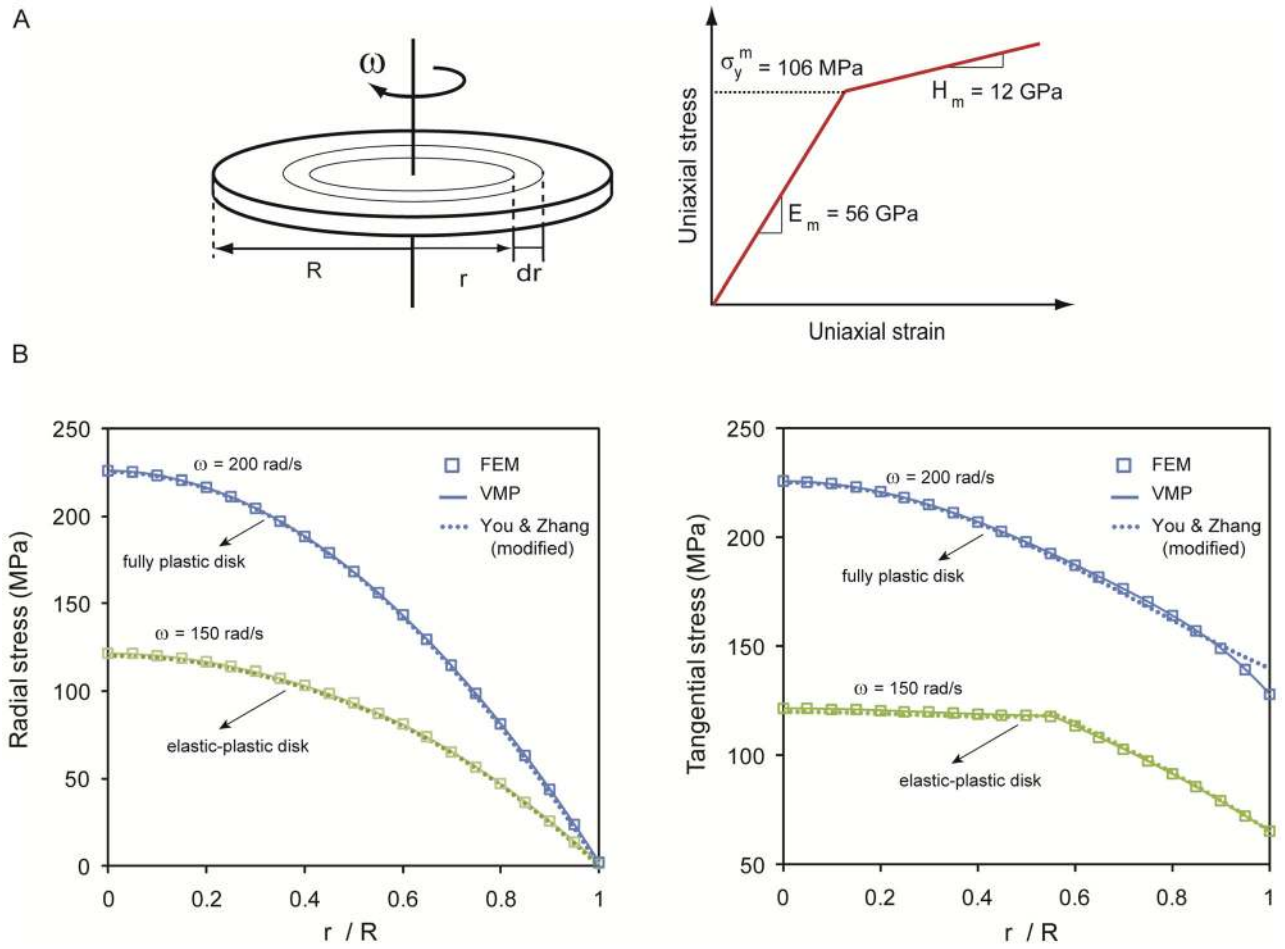

Fig. 1 (*a*) Schematic of a thin rotating disk and the bilinear stress–strain curve of the disk material (metal). (*b*) Distribution of radial and tangential stresses in an all metal rotating disk at $\omega = 150$ and 200 rad/s. For the angular velocity $\omega = 150$ rad/s, the disk deforms plastically at the inner part and is elastic close to the outer edge. For $\omega = 200$ rad/s, the disk deforms plastically along its radius. The radius of the disk is 120 cm and the metal density is considered 10^4 kg/m^3.

stresses inside the rotating disk. The conclusions are drawn in Sec. 5.

2 Theoretical Model

In the development of the model, it was assumed that the metal–ceramic composite is locally isotropic and yields according to the von Mises criterion. The axisymmetric structure (here a thin disk) is divided into infinitesimally small axisymmetric thin rings. A ring located at distance r from the disk center—see Fig. 1(*a*)—has the elastic modulus, $E(r)$, Poisson ratio $v(r)$, and is assigned an effective stress–strain curve that represents the plastic behavior of the ring material. The component of the strain tensor in the ring, ε_{ij}, is the summation of the elastic part, ε_{ij}^e and plastic part, ε_{ij}^p. The elastic part is given as, $\varepsilon_{ij}^e = \frac{1+v(r)}{E(r)}\sigma_{ij} - \frac{v(r)}{E(r)}\sigma_{kk}\delta_{ij}$, where δ_{ij} is the Kronecker delta. The plastic part of strain is given by Hencky's total deformation equation, $\varepsilon_{ij}^p = \phi(r)s_{ij}$, where $s_{ij} = \sigma_{ij} - \frac{1}{3}\sigma_{kk}\delta_{ij}$ is the deviatoric stress, and ϕ is a scalar function given by $\phi = 3\varepsilon^{-p}/2\sigma_{\text{eq}}$, where ε^{-p} and σ_{eq} are the equivalent plastic strain and equivalent stress, respectively. Considering the above relationships, the total strain in the element can be written as

$$\varepsilon_{ij} = \left(\frac{1+v(r)}{E(r)} + \phi(r)\right)\sigma_{ij} - \left(\frac{v(r)}{E(r)} + \frac{1}{3}\phi(r)\right)\sigma_{kk}\delta_{ij} \quad (1)$$

Now, we assume an equivalent *elastic element* located at x, with an effective elastic modulus and an effective Poisson ratio, denoted by $E_{\text{eff}}(r)$ and $v_{\text{eff}}(r)$, respectively. This element has elastic strain components equal to the total strain components of the elasto-plastic element presented in Eq. (1). The component of strain tensor in this hypothetical elastic element, ε_{ij}^*, is

$$\varepsilon_{ij}^* = \frac{1+v_{\text{eff}}(r)}{E_{\text{eff}}(r)}\sigma_{ij} - \frac{v_{\text{eff}}(r)}{E_{\text{eff}}(r)}\sigma_{kk}\delta_{ij} \quad (2)$$

comparing Eqs. (3) and (4) and eliminating $\phi(r)$ from the above equations gives

$$v_{\text{eff}}(r) = \frac{E_{\text{eff}}(r)(2v(r)-1) + E(r)}{2E(r)} \quad (3)$$

In the analysis, first $E_{\text{eff}}(r) = E(r)$ and $v_{\text{eff}}(r) = v(r)$ for each element. Considering all elements to satisfy the requirements of equilibrium and compatibility at their boundary (i.e., interface with adjacent elements), the state of elastic stress in the thin rotating disk was evaluated in each step using Lame's equations for each elastic strip [34]. For a thin strip located at x, the inside and outside displacements, u_1 and u_2, are related to the inside and outside pressures, p_1 and p_2, by the following relations

$$\begin{Bmatrix} u_1 \\ u_2 \end{Bmatrix} = \begin{bmatrix} C_{11} & C_{12} \\ C_{21} & C_{22} \end{bmatrix} * \begin{Bmatrix} p_1 \\ p_2 \end{Bmatrix} + \begin{Bmatrix} k_1 \\ k_2 \end{Bmatrix} \tag{4}$$

where in the plane stress case

$$C_{11,r} = \frac{1+\nu_{\text{eff}}(r)}{E_{\text{eff}}(r)} \frac{r^3}{(r+dr)^2 - r^2} \left(\frac{1-\nu_{\text{eff}}(r)}{1+\nu_{\text{eff}}(r)} + \frac{(r+dr)^2}{r^2} \right)$$

$$C_{12,r} = \frac{-2}{E_{\text{eff}}(r)} \frac{r(r+dr)^2}{(r+dr)^2 - r^2}$$

$$C_{21,r} = \frac{2}{E_{\text{eff}}(r)} \frac{(r+dr)r^2}{(r+dr)^2 - r^2}$$

$$C_{22,r} = -\frac{1+\nu_{\text{eff}}(r)}{E_{\text{eff}}(r)} \frac{(r+dr)^3}{(r+dr)^2 - r^2} \left(\frac{1-\nu_{\text{eff}}(r)}{1+\nu_{\text{eff}}(r)} + \frac{r^2}{(r+dr)^2} \right)$$

and

$$K_1 = \frac{\rho(r) * \omega^2 * (1-\nu_{\text{eff}}(r))^2}{8E_{\text{eff}}(r)} * \left(\frac{3+\nu_{\text{eff}}(r)}{1+\nu_{\text{eff}}(r)} + (r^2 + (r+dr)^2) * r + \frac{3+\nu_{\text{eff}}(r)}{1-\nu_{\text{eff}}(r)} * (r+dr)^2 r - r^3 \right)$$

$$K_2 = \frac{\rho(r) * \omega^2 * (1-\nu_{\text{eff}}(r))^2}{8E_{\text{eff}}(r)} * \left(\frac{3+\nu_{\text{eff}}(r)}{1+\nu_{\text{eff}}(r)} + (r^2 + (r+dr)^2) * (r+dr) + \frac{3+\nu_{\text{eff}}(r)}{1-\nu_{\text{eff}}(r)} * r^2(r+dr) - (r+dr)^3 \right) \tag{5}$$

where r and $(r+dr)$ are the inner and outer radii of the strip. After assembling all strips together, a system of linear equations of the form $[C']\{U\} = \{P\} + \{K'\}$ is obtained, where $\{U\}$ is the radial displacement vector of the strips at their interface, $\{P\}$ is the interfacial pressure vector, and $\{K'\}$ is the matrix denoting the contribution of the inertia. Solving this equation gives $\{U\}$.

Next, $E_{\text{eff}}(r)$ is updated by applying the projection method for each element based on the calculated equivalent (von Mises) stress [33] (i.e., $E_{\text{eff}}(r) = \frac{\sigma(\varepsilon_{\text{eff}})}{\varepsilon_{\text{eff}}}$, where the function $\sigma(\varepsilon)$ represents the effective stress–strain curve of the material at distance r). The effective Poisson ratio for each element, $\nu_{\text{eff}}(r)$, is obtained using Eq. (3). In the next step, the state of stress in each element is recalculated using the updated values of effective elastic modulus and effective Poisson's ratio. This procedure is continued until the convergence to the stress solution is achieved.

Several models have been proposed for estimating the linear and nonlinear response of particulate composites, which are capable of predicting the effective mechanical properties of the composite material with high fidelity for relatively simple microstructures or low volume fraction of one of the constituents [35–41]. More complex models of materials with varying elastic and plastic properties have taken into consideration the effect of material gradation, microstructure, and the interactions between the material constituents [42–48]. Here, we assumed that the metal matrix has bilinear elastic–plastic behavior with density, ρ_m, elastic modulus, E_m, tangent modulus, H_m, and yield stress, σ_y^m. The ceramic was assumed to have density, ρ_c, and be linear elastic with elastic modulus, E_c. We estimated the material properties of the metal–ceramic composite (density, ρ_{mc}; elastic modulus, E_{mc}; overall flow strength of the composite corresponding to the onset of yielding, σ_y^{mc}; tangent modulus of the composite representing its strain hardening behavior, H_{mc}) using the modified rule of mixture for composites [49]

$$\rho_{mc} = (1-f)\rho_m + f\rho_c$$

$$E_{mc} = \left[(1-f)\left(\frac{q+E_c}{q+E_m} \right) + f \right]^{-1} * \left[(1-f)E_m \left(\frac{q+E_c}{q+E_m} \right) + fE_c \right]$$

$$\sigma_y^{mc} = \sigma_y^m \left[(1-f) + \left(\frac{q+E_m}{q+E_c} \right) \cdot \frac{E_c}{E_m} \cdot f \right]$$

$$H_{mc} = \left[(1-f)\left(\frac{q+E_c}{q+H_m} \right) + f \right]^{-1} * \left[(1-f)H_m \left(\frac{q+E_c}{q+H_m} \right) + fE_c \right] \tag{6}$$

where f denotes the volume fraction of the ceramic particles and q is the so called stress to strain transfer ratio, a parameter which is independent of f and defines the metal/ceramic interface behavior [49].

In all the calculations presented here, the metal component of the FG material has $E_m = 56$ GPa, $H_m = 12$ GPa, $\sigma_y^m = 106$ MPa, density $\rho_m = 10^4$ kg/m^3, and the Poisson ratio is assumed to be constant and equal to 0.25 [50]. The density and elastic modulus of ceramic were varied systematically in the ranges of ~5 GPa–560 GPa (i.e., $0.1 < E_c/E_m < 10$) and 10^2 kg/m^3–10^4 kg/m^3 (i.e., $0.1 < \rho_c/\rho_m < 10$), respectively. The values of ceramic density and ceramic modulus of elasticity $\rho_c = 10^4$ kg/m^3 and $E_c = 80$ GPa were taken in the calculations as default, respectively. The ceramic Poisson's ratio was considered to be 0.25. The value of q is taken as 17.2 GPa based on the micro-indentation experiments by Gu et al. [50].

To account for a wide range of possible distribution patterns of ceramic particles, two different power-law distributions for the ceramic volume fraction were considered:

(i) A rotating disk with a monotonic increase in the ceramic volume fraction from 0 at its center to f_o at the outer radius

$$f_c(r) = f_o \left(\frac{r}{R} \right)^n \quad 0 \le f_o \le 1, \quad n > 0 \tag{7}$$

where R is the disk radius, $f_c(r)$ is the ceramic volume fraction at distance r from the disk center, and n is the exponent of the ceramic volume fraction distribution function. (ii) A rotating disk with a monotonic decrease in the ceramic volume fraction from f_i at its center to 0 at the outer radius.

$$f_c(r) = f_i \left(\frac{R-r}{R} \right)^n \quad 0 \le f_i \le 1, \quad n > 0 \tag{8}$$

$f_o = 0$ in Eq. (1) and $f_i = 0$ in Eq. (2) denote a metallic disk and $n = 0$ in both equations denotes a uniformly reinforced metal–ceramic disk.

3 Stresses in a Uniform Rotating Disk

Figure 1 shows the stresses distribution in a uniform elasto-plastic rotating disk obtained from three different methods, namely, finite element analysis, a modified form of the semi-analytical method introduced by You and Zhang [1], and the VMP method outlined in Sec. 2. The material is considered to behave according to a bilinear stress–strain curve (e.g., linear strain hardening behavior) with the properties shown in Fig. 1(*a*).

The analytical method proposed by You and Zhang [1] is based on the assumption that the stresses induced in a solid uniform rotating disk of constant thickness can be estimated by a polynomial of the even powers of radius r. The polynomial terms are obtained by satisfying the requirement of compatibility and equilibrium. For a rotating disk made of a material with linear strain hardening in the plastic regime, however, the method presented in Ref. [1] does not show a good agreement with the results obtained

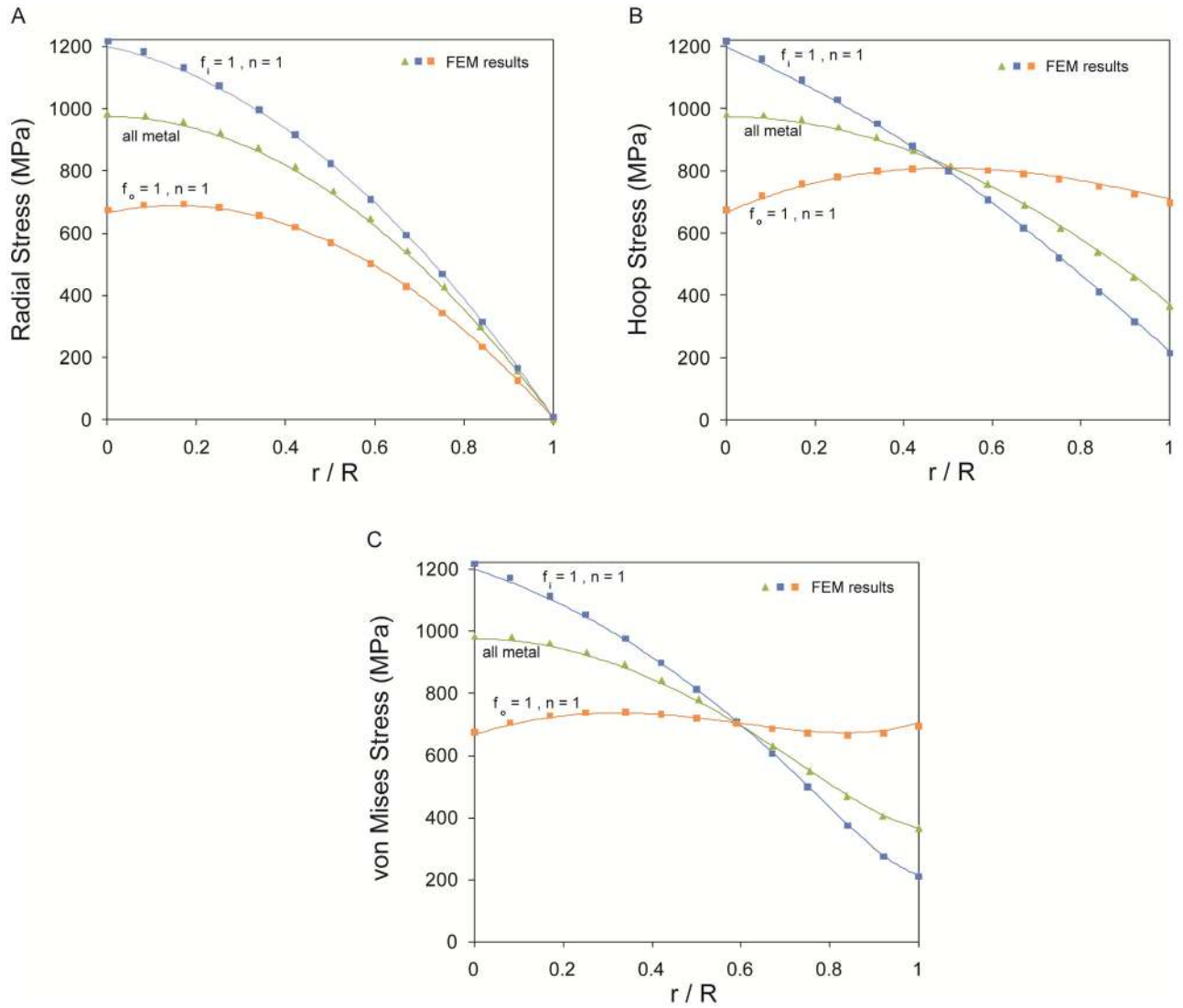

Fig. 2 Distribution of (*a*) radial, (*b*) hoop, and (*c*) von Mises stresses for a FG metal–ceramic rotating disk subjected to $\omega = 400$ rad/s for different reinforcement distributions. The radius of the disk is 120 cm.

from the finite element analysis. To enhance the accuracy of the method, You and Zhang estimated the linear strain hardening behavior with a nonlinear, polynomial form of stress–plastic strain curve at small plastic strains.

We have re-evaluated the work by You and Zhang and noticed that the error in the results for a linear strain hardening behavior can be avoided by simplifying the boundary conditions of governing equation. This simplification results in a significant reduction of the complexity of the equations that should be solved and the associated numerical errors. The details of the modified solution method are presented in Appendix. The radial stress distributions obtained from the three methods show a good agreement for both elasto-plastic and fully plastic disks, Fig. 1(*c*). However, the modified You and Zhang method could not predict the tangential stresses close to the outer edge of the disk with high fidelity. According to the results shown, the VMP method is capable of predicting stresses in both elasto-plastic and fully plastic disks with high fidelity.

4 Stresses in a FG Rotating Disk

In Fig. 2, the distribution of the principal and von Mises stresses in a FG disk with a linear decrease in the ceramic content in the radial direction ($f_i = n = 1$) and a FG disk with a linear increase in the ceramic content in the radial direction ($f_o = n = 1$) are plotted and compared to the stress distribution in a uniform metal disk for an angular velocity of $\omega = 400$ rad/s. At this angular velocity, entire sections of the three disks undergo plastic deformation. Finite element results are also presented for these cases. For finite element modeling of the FG rotating disk, the thin disk was divided into 50 axisymmetric, concentric rings, and each ring was assigned with a material property associated with the material property of the material at the midradius of the ring using Eq. (6). The model was meshed using two-dimensional, eight-node quadrilateral elements and mesh sensitivity analysis was performed to assure that the results are not sensitive to the ring size or meshing. The results obtained from the developed method show excellent agreement with the finite element calculations. The advantage of the proposed method over the finite elements analysis is the computational simplicity and efficiency for parametric and optimization studies.

The disk with $f_o = n = 1$ has the lowest stress at the center and develops relatively uniform hoop and von Mises stress distributions. In contrast, the disk with $f_i = n = 1$ has higher stresses at its center compared to the uniform (all metal) disk and a strongly nonuniform stress distribution. Further analysis of a FG rotating

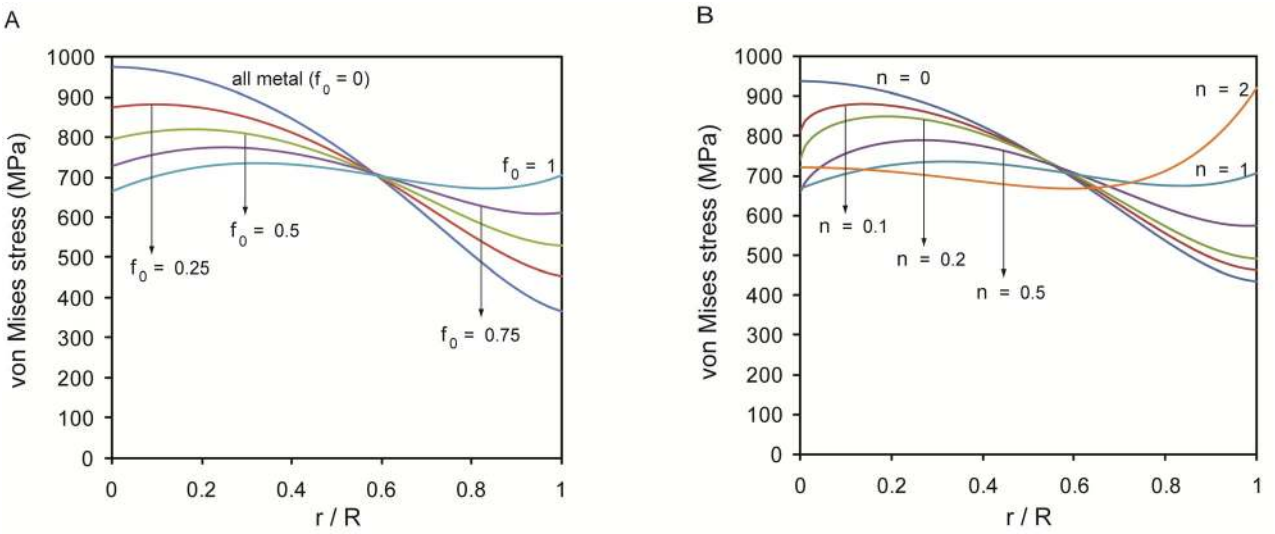

Fig. 3 (*a*) Distribution of von Mises stress in a FG rotating disk with $n = 1$ and different values of f_o. (*b*) von Mises stress induced in the FG rotating disk with $f_o = 1$ and different values of n. The disk is rotating at $\omega = 400$ rad/s.

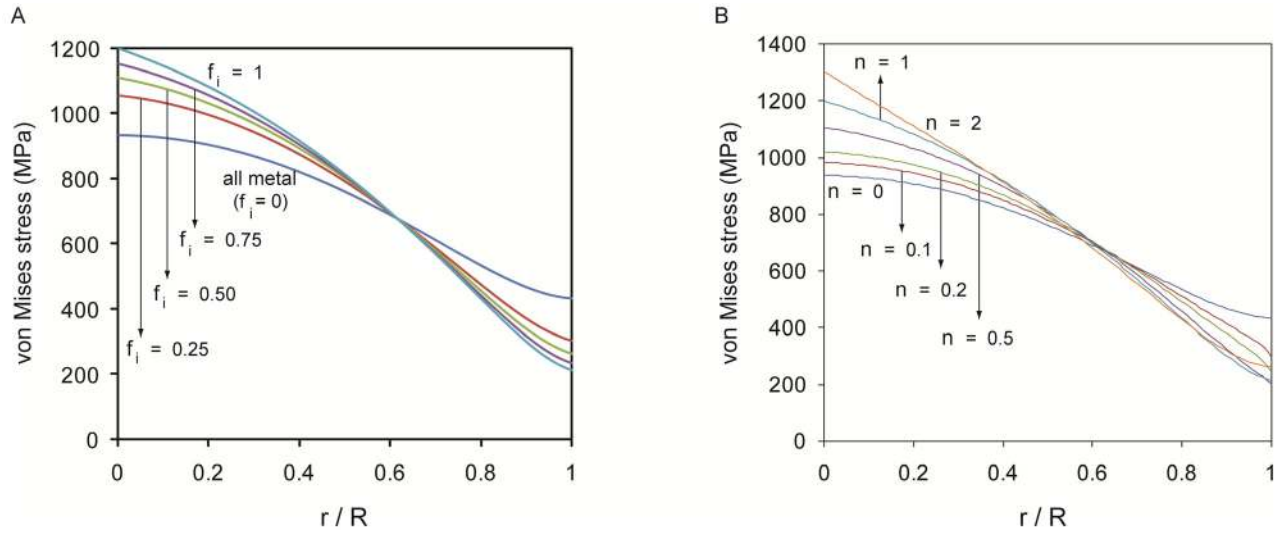

Fig. 4 (*a*) Distribution of von Mises stress in a FG rotating disk with $n = 1$ and different values of f_i. (*b*) von Mises stress induced in the FG rotating disk with $f_i = 1$ and different values of n. The disk is rotating at $\omega = 400$ rad/s.

disk with a radially increasing ceramic content (that increases from the disk center to outer radius) is presented in Fig. 3. The results are obtained by systematically changing the values of ceramic content at the outer radius, f_o, and ceramic distribution coefficient, n. Only von Mises stresses are plotted assuming that the failure is mainly related to the excessive value of the von Mises stress. Increasing f_o results in a near constant stress distribution and reduces the maximum value of the von Mises stress in the disk. The disk with $f_o = 1$ has near-uniform stress distribution with the maximum von Mises stress occurring at $r/R = 0.33$. In Fig. 3(*b*), we analyzed the stress distribution in a rotating disk with $f_o = 1$ and different distribution exponents. Increasing the value of $n$from 0 to 1 results in a reduction in the maximum von Mises stress. However, further increase in the values of n results in a stress concentration at the outer edge of the rotating disk. Further analysis showed that for a given distribution, the linear increase in the ceramic content provides the most evenly distributed stresses in the disk. We have regenerated a similar set of results for a disk with radially decreasing ceramic content. The results are summarized in Fig. 4. For all FG disks (i.e., all values of f_i and n), the von Mises stress is maximum at the center of the disk and its values increases by increasing f_i or n.

To understand the significance of the density and elastic modulus of the material constituents of a rotating disk on the stress distributions, we carried out a parametric study by changing each of these parameters systematically. Figure 5 shows the results obtained by changing the ceramic density, ρ_c, while the metal density is kept constant, $\rho_m = 10^4$ kg/m^3, for a rotating disk with $f_o = 1$ and $n = 1$. In Fig. 5(*a*), the distribution of the von Mises stress is plotted for $\rho_c/\rho_m = 0.5$, 2, 5, and 10 for an angular velocity $\omega = 200$ rad/s. The plastic zone initiates from the center in this set of calculations. Increasing the ceramic density increases the von Mises stresses along the radius of the disk due to an increase in the inertia body forces. In this set of calculations, the disk deforms elastically for $\rho_c/\rho_m = 0.5$ and is fully plastic for all other cases. The locus of elastic and plastic regions in a rotating

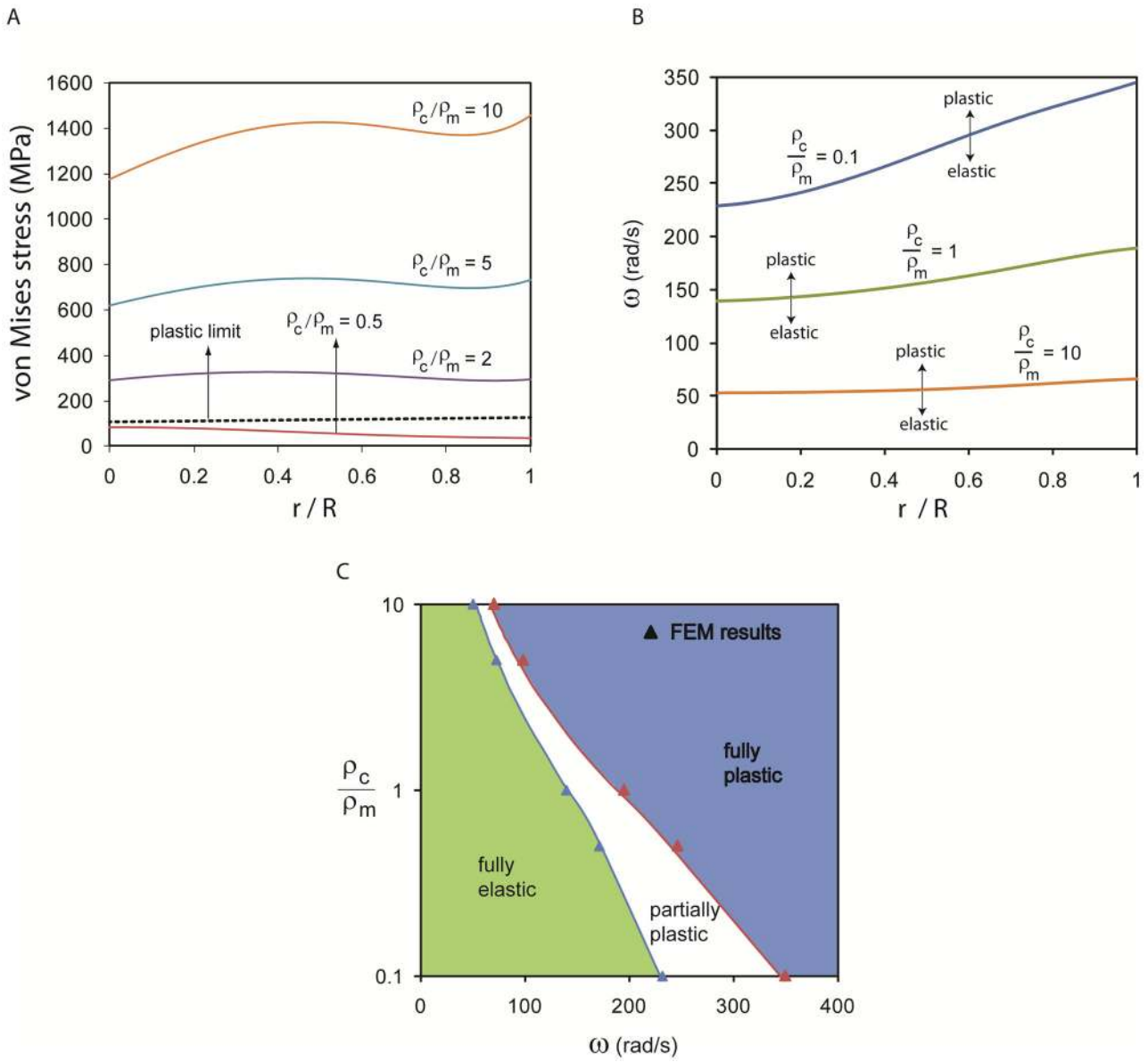

Fig. 5 (*a*) Effect of relative density of ceramic and metal, ρ_c/ρ_m, on the distribution of von Mises stress in a FG rotating disk subjected to $\omega = 200$ rad/s. (*b*) The locus of elastic and plastic regions in a FG disk at different angular velocities for three values of ρ_c/ρ_m. (*c*) Relative density of ceramic and metal, ρ_c/ρ_m, versus the angular velocities developing incipient and full plasticity in a FG disk. The ceramic volume fraction varies according to $f_c(r) = (r/R)$ in these sets of results.

disk according to the angular velocity is depicted in Fig. 5(*b*) for different ceramic to metal density ratio, ρ_c/ρ_m. For each curve corresponding to a specific metal to ceramic density ratio, the sections below and above the curve at every angular velocity present the regions of elastic and plastic deformation in the disk, respectively. For example, for a disk with $\rho_c/\rho_m = 1$ and subjected to $\omega = 300$ rad/s, the inner region of $0 < r/R < 0.63$ deforms plastically, while the disk deforms elastically in $0.63 < r/R < 1$. The map showing the occurrence of fully elastic, partially plastic, and fully plastic disks according to the ceramic to metal density ratio and disk angular velocity is displayed in Fig. 5(*c*). By increasing the ceramic density, the plasticity initiates in the disk at a lower angular velocity. The angular velocity range for which the disk deformation is partially plastic becomes narrower by increasing the ceramic relative density.

The role of ceramic to metal elastic modulus ratio, E_c/E_m, in a rotating disk with $f_o = 1$ and $n = 1$ is investigated in Fig. 6. In this set of calculations, the elastic modulus of the metal was kept constant, while the ceramic elastic modulus was changed in the range of $0.1 < E_c/E_m < 10$. By increasing the ceramic elastic modulus, the von Mises stress distribution pattern changes from radially decreasing to an almost uniform distribution along the radius of the disk, and then radially increasing by further increasing the E_c/E_m value. The optimum value of the modulus of elasticity ratio is obtained as $E_c/E_m = 2$ corresponding to the most uniform von Mises stress distribution with the least difference between the minimum and maximum stress along the radius of the FG disk. The locus of elastic and plastic regions in a rotating disk according to the angular velocity is shown in Fig. 6(*b*) for different E_c/E_m. For each curve corresponding to a specific metal to ceramic modulus of elasticity ratio, the sections below and above the curve at every angular velocity represent the regions of elastic and plastic deformation in the disk, respectively. For example, for a disk with $E_c/E_m = 10$ and subjected to $\omega = 250$ rad/s the inner region of $0 < r/R < 0.35$ deforms plastically, while the disk deforms elastically in $0.35 < r/R < 1$. Interestingly, in all the cases

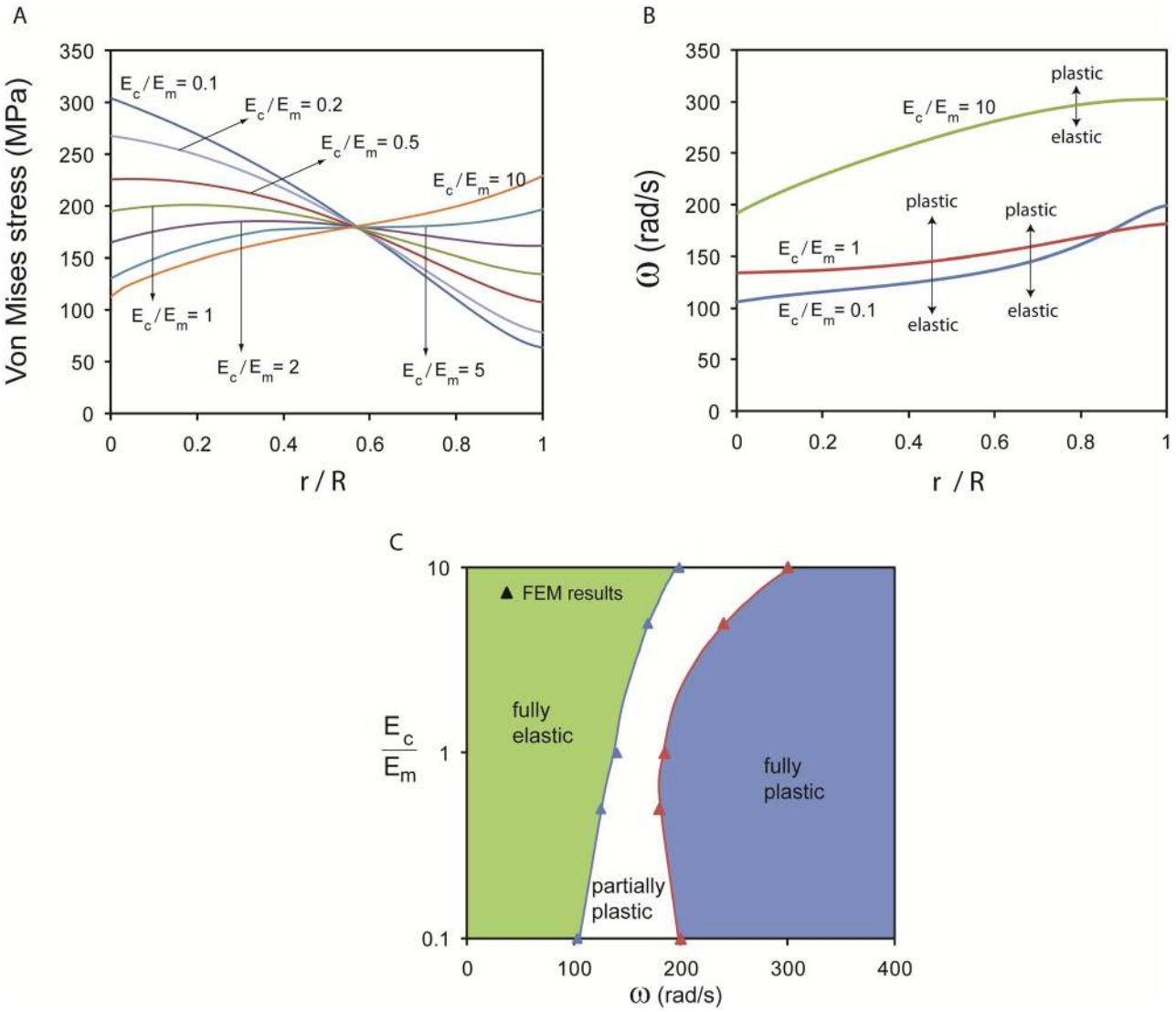

Fig. 6 (*a*) Effect of relative stiffness of ceramic and metal, E_c/E_m, on the distribution of von Mises stress in a FG rotating disk subjected to $\omega = 200$ rad/s. (*b*) The locus of elastic and plastic regions in a FG disk at different angular velocities for three values of E_c/E_m. (*c*) Relative stiffness of ceramic and metal, E_c/E_m, versus the angular velocities developing incipient and full plasticity in a FG disk. The ceramic volume fraction varies according to $f_c(r) = (r/R)$ in these sets of results.

included in these results the plastic deformation initiates from the center of the disk. This is despite the fact that the value of stresses is higher at the outer edge of the disk compared to its center for several cases (e.g., $E_c/E_m = 10$). The reason is that the yield stress of the disk material varies along its radius depending on the volume fraction of the ceramic, which is changed linearly in this case. The map showing the occurrence of fully elastic, partially plastic, and fully plastic disk according to the values of ceramic to metal elastic modulus ratio and angular velocity of the disk is shown in Fig. 6(*c*). By increasing the ratio of modulus of elasticity, the critical angular velocity corresponding to incipient plasticity monotonically increases, whereas the critical angular velocity corresponding to full plasticity of the disk decreases slightly in the $0.1 < E_c/E_m < \sim 1$ range and then increases by increasing the ceramic elastic modulus.

A similar set of calculations were carried out for disks with radially decreasing ceramic content ($f_i = 1$, $n = 1$) and the results are summarized in Fig. 7. The distribution of von Mises stress in disks with different ceramic to metal elastic modulus ratios, E_c/E_m, is shown in Fig. 7(*a*). By decreasing the E_c/E_m value from 10 to 0.1, the von Mises stress distribution pattern changes from radially decreasing to a near-uniform distribution along the radius of the disk. In contrast to a uniform disk and FG disk with radially increasing ceramic content, the plasticity does not necessarily initiate from the center in a rotating FG disk with radially decreasing ceramic content. In fact, the locus of the incipient plasticity depends on the distribution of material properties inside the disk and the disk thickness profile. In Fig. 7(*b*), we have shown the distribution of von Mises stresses inside the disk for different angular velocities. The yield stress of the disk changes linearly according to Eq. (1) and is shown by dashed line in this figure. The plastic region is found by comparing the local equivalent stress with the plastic limit of the local material. At $\omega = 112$ (rad/s), the von Mises stress at the outer radius of the disk first reaches the corresponding yielding stress of that radius. By increasing the angular velocity to 138 (rad/s), both the outer radius and the center of the disk become plastic, and the middle part of the disk becomes elastic. At $\omega = 145$ (rad/s), the entire disk undergoes plastic deformation. The locus of elastic and plastic regions in the disk according to angular velocity of the disk is depicted in Fig. 7(*c*) for different modulus of elasticity ratios, E_c/E_m. It is shown that in the FG rotating disks, the plasticity can initiate from the outer radius,

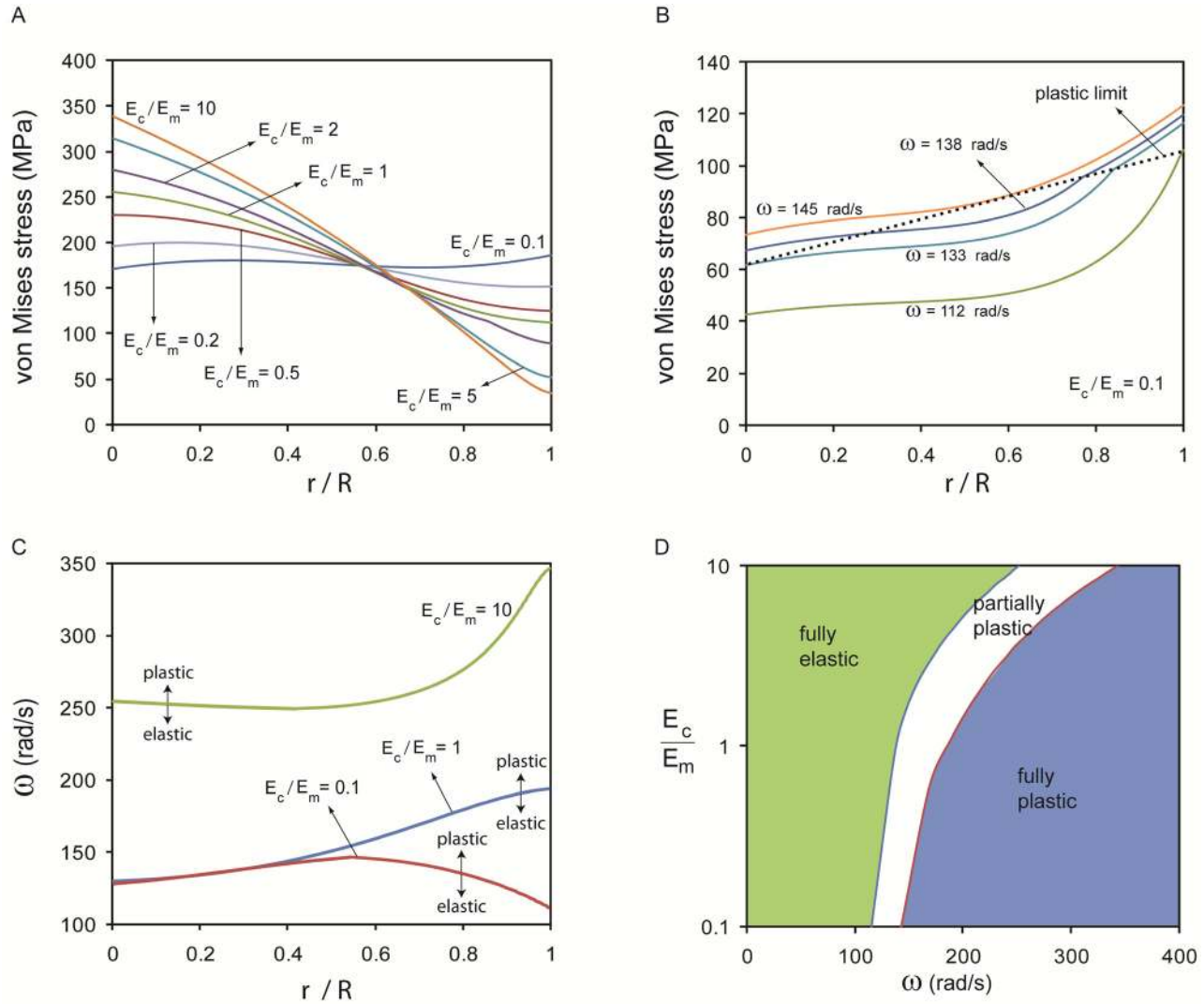

Fig. 7 (*a*) Effect of relative stiffness of ceramic and metal, E_c/E_m, on the distribution of von Mises stress in a FG rotating disk subjected to $\omega = 200$ rad/s. (*b*) The von Mises stress distribution in a rotating disk with $E_c/E_m = 0.1$ subjected to four different angular velocities. (*c*) The locus of elastic and plastic regions in a FG disk at different angular velocities for three values of E_c/E_m. (*d*) Relative stiffness of ceramic and metal, E_c/E_m, versus the angular velocities developing incipient and full plasticity in a FG disk. The ceramic volume fraction varies according to $f_c(r) = (1 - r/R)$ in these sets of results.

middle section, or center of the disk depending on different reinforcement distributions and/or reinforcement properties. For instance, by increasing the angular velocity in initially fully elastic disks with E_c/E_m of 0.1, 1, and 10, the plastic zone is initiated from the outer radius, center, and middle section of the disk, respectively. The map showing the occurrence of fully elastic, partially plastic, and fully plastic disks according to the values of ceramic to metal elastic modulus ratio and angular velocity of the disk is given in Fig. 7(*d*). By increasing the modulus of elasticity ratio the critical angular velocity corresponding to incipient and full plasticity of the disk increases nonlinearly.

To illustrate the capability of the proposed method in optimization and parametric studies of the elastic–plastic rotating disk problem, we have obtained the optimized distribution of the ceramic particles leading to the minimum outer edge displacement in a FG rotating disk. The distribution of the ceramic through the radius of disk was changed by varying the n and f parameters in Eqs. (1) or (2). The average volume fraction of ceramic is obtained by integrating the ceramic volume fraction over the radius and dividing it by the disk volume. For a disk with a radially increasing ceramic content, $f_{\text{ave}} = \frac{2}{n+2} * f_o$. For a disk with a decreasing ceramic content, $f_{\text{ave}} = \frac{2}{n^2+3n+2} * f_i$.

The disk outer edge displacement normalized by disk radius versus the average volume fraction of ceramic constituent in a disk with $\omega = 400$ rad/s and different reinforcement distribution coefficients f_o is obtained and is shown in Fig. 8(*a*). The outer edge displacement is minimum when $n = 0$ in Eq. (7), implying that within disks with constant or increasing ceramic content in the radial direction the uniform ceramic particle distribution yields the minimum radial plastic expansion. For disks with radially decreasing ceramic content according to Eq. (8) and $\omega = 400$ rad/s, the normalized outer edge displacement is plotted versus the average ceramic volume fraction in Fig. 8(*b*). In disks with increasing ceramic content toward the center, whenever the value of ceramic average volume fraction is greater than 0.3 the disk with $f_i = 1$ yields the minimum outer edge displacement. When the average value is less than 0.3, the outer edge displacement in a disk with $f_i = f_{\text{opt}} < 1$ is minimum. However, the difference between the displacements in disks with the $f_i = f_i^{\text{opt}}$ and $f_i = 1$ is relatively small.

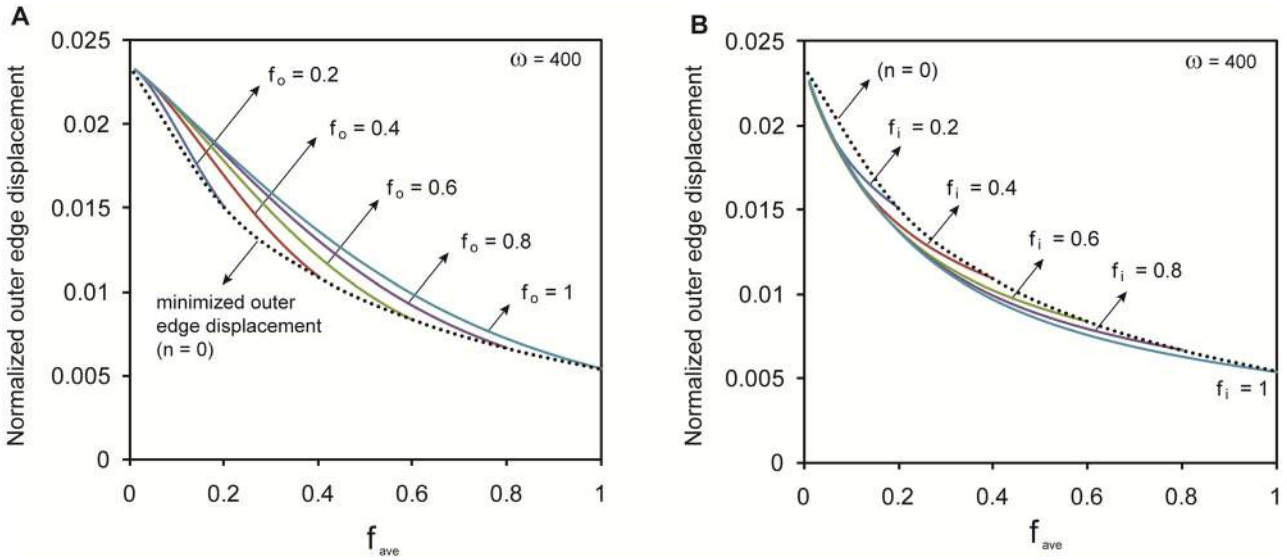

Fig. 8 (*a*) The normalized outer edge displacement versus the average ceramic volume fraction for FG disks of radially increasing volume fraction with different reinforcement coefficients f_o according to Eq. (7). (*b*) The normalized outer edge displacement versus the average ceramic volume fraction for FG disks of radially decreasing volume fraction with different reinforcement coefficients f_i according to Eq. (8). The disks are subjected to $\omega = 400$ rad/s.

5 Conclusion

The elasto-plastic stress field in a FG rotating disk was obtained using an extended VMP method and was used to analyze metal–ceramic rotating disks with different ceramic particle distributions. Our work suggests that reinforcement of metal disks with ceramic particles can significantly influence the mechanical response of the disk such as the critical angular velocity corresponding to the onset of and full plasticity, as well as the distribution of stresses in the disk. It was shown that in a FG disk, the plastic deformation does not essentially initiate from the center of the rotating disk and might originate at the outer edge or the middle section of the disk. These cases were shown to happen for disks with decreasing ceramic content through the radius of the disk and different ceramic to metal ratios of elastic modulus. Also, it was shown that disks with an increasing ceramic content toward the outer edge have a more uniform stress distribution. This was expected since typically higher stresses are developed in regions of higher stiffness in a composite structure (i.e., in our case, regions with a high ceramic volume fraction) as compared to the uniform, elastic structure under the same loading condition. As an example of the application of the proposed method, different power-law ceramic volume fraction distributions were compared to obtain the optimum reinforcement distribution that leads to the minimized outer edge displacement. It was shown that by increasing the ceramic content in the central region of the disk, the outer edge displacement of the disk decreases. Although our parametric study does not offer a general conclusion for selecting the optimum material configuration for a particle reinforced rotating disk, it does provide enough insight for selecting the near-optimized reinforced configurations.

Acknowledgment

This work was supported by NSF—CMMI 1065759.

Appendix

The governing equation for an elastic–plastic uniform rotating disk in terms of the stress function φ (yielding radial and hoop stresses as $\sigma_r = \frac{\varphi}{r}$ and $\sigma_\theta = \frac{d\varphi}{dr} + \rho\omega^2 r^2$ and the plastic strain in radial and circumferential directions) is [1]

$$r\frac{d^2\varphi}{dr^2} + \frac{d\varphi}{dr} - \frac{\varphi}{r} + (3+\nu)\rho\omega^2 r^2 + E\left(r\frac{d\varepsilon_\theta^p}{dr} + \varepsilon_\theta^p - \varepsilon_r^p\right) = 0 \tag{A1}$$

You and Zhang assumed an infinite polynomial of the even powers of radius as the analytical solution of the stress function for a solid rotating disk (see Ref. [1] for the justification), which can be presented as

$$\varphi = \sum_{n=1}^{N} c_{2n-1} r^{2n-1} = c_1 r + c_3 r^3 + c_5 r^5 + c_7 r^7 + \cdots \tag{A2}$$

where c_{2n-1} are constants. Thus, the radial and tangential stresses are obtained according to the stress function

$$\sigma_r = \frac{\varphi}{r} = c_1 + c_3 r^2 + c_5 r^4 + c_7 r^6 + \cdots$$
$$\sigma_\theta = \frac{d\varphi}{dr} + \rho\omega^2 r^2 = c_1 + (3c_3 + \rho\omega^2) r^2 + 5c_5 r^4 + 7c_7 r^6 + \cdots \tag{A3}$$

and the equivalent stress is obtained as

$$\sigma_e = \sqrt{\sigma_r^2 + \sigma_\theta^2 - \sigma_r\sigma_\theta} = c_1\sqrt{1 + a_2 r^2 + a_4 r^4 + a_6 r^6} \tag{A4}$$

Where

$$a_2 = \frac{4c_1c_3 + c_1\rho\omega^2}{c_1^2}$$
$$a_4 = \frac{7c_3^2 + 6c_1c_5 + 5c_3\rho\omega^2 + \rho^2\omega^4}{c_1^2}$$
$$a_6 = \frac{8c_1c_7 + 24c_3c_5 + 9c_5\rho\omega^2}{c_1^2} \tag{A5}$$

The relations between the stresses and plastic strains for the plane stress problem according to the deformation theory of plasticity may be written as

$$\varepsilon_r^p = \frac{\varepsilon_e^p}{\sigma_e}\left(\sigma_r - \frac{1}{2}\sigma_\theta\right) \quad \varepsilon_\theta^p = \frac{\varepsilon_e^p}{\sigma_e}\left(\sigma_\theta - \frac{1}{2}\sigma_r\right) \tag{A6}$$

The equivalent stress and plastic strain are assumed to have a *linear* relation as $\varepsilon_e^p = a_1\sigma_e + a_0$. Substitution into Eq. (A6) yields

$$\varepsilon_r^p = \left(a_1 + \frac{a_0}{\sigma_e}\right)\left(\sigma_r - \frac{1}{2}\sigma_\theta\right) \quad \varepsilon_\theta^p = \left(a_1 + \frac{a_0}{\sigma_e}\right)\left(\sigma_\theta - \frac{1}{2}\sigma_r\right) \tag{A7}$$

expressing the term $\frac{1}{\sigma_e}$ in Eq. (A7) according to the even powers of r using the Taylor series expansion yields

$$\frac{1}{\sigma_e} = \frac{1}{c_1}(1 + b_2 r^2 + b_4 r^4 + b_6 r^6) \tag{A8}$$

where

$$b_2 = -\frac{a_2}{2}$$
$$b_4 = \frac{3}{8}a_2^2 - \frac{a_4}{2}$$
$$b_6 = -\frac{45}{144}a_2^3 + \frac{3}{4}a_2 a_4 - \frac{a_6}{2} \tag{A9}$$

The plastic strain components now may be written as the following polynomials

$$\varepsilon_r^p = \varepsilon_{r0}^p + \varepsilon_{r2}^p r^2 + \varepsilon_{r4}^p r^4 + \varepsilon_{r6}^p r^6 + \cdots$$
$$\varepsilon_\theta^p = \varepsilon_{\theta 0}^p + \varepsilon_{\theta 2}^p r^2 + \varepsilon_{\theta 4}^p r^4 + \varepsilon_{\theta 6}^p r^6 + \cdots \tag{A10}$$

where ε_{ri}^p, $\varepsilon_{\theta i}^p$ $(i = 0,2,4,6,...)$ in Eq. (A10) are obtained from Eqs. (A3), (A7), and (A8) as follows:

$$\varepsilon_{r0}^p = \left(a_1 + \frac{a_0}{c_1}\right)\frac{c_1}{2}$$
$$\varepsilon_{r2}^p = \left(a_1 + \frac{a_0}{c_1}\right)\left(-\frac{c_3}{2} - \frac{\rho\omega^2}{2}\right) + \frac{a_0 b_2}{2}$$
$$\varepsilon_{r4}^p = \left(a_1 + \frac{a_0}{c_1}\right)\left(-\frac{3c_5}{2}\right) + \left(\frac{a_0 b_2}{c_1}\right)\left(-\frac{c_3}{2} - \frac{\rho\omega^2}{2}\right) + \frac{a_0 b_4}{2}$$
$$\varepsilon_{r6}^p = \left(a_1 + \frac{a_0}{c_1}\right)\left(-\frac{5c_7}{2}\right) + \left(\frac{a_0 b_2}{c_1}\right)\left(-\frac{3c_5}{2}\right) + \left(\frac{a_0 b_4}{c_1}\right)\left(-\frac{c_5}{2} - \frac{\rho\omega^2}{2}\right) + \frac{a_0 b_6}{2}$$
$$\varepsilon_{\theta 0}^p = \left(a_1 + \frac{a_0}{c_1}\right)\frac{c_1}{2}$$
$$\varepsilon_{\theta 2}^p = \left(a_1 + \frac{a_0}{c_1}\right)\left(\frac{5c_3}{2} + \rho\omega^2\right) + \frac{a_0 b_2}{2}$$
$$\varepsilon_{\theta 4}^p = \left(a_1 + \frac{a_0}{c_1}\right)\left(\frac{9c_5}{2}\right) + \left(\frac{a_0 b_2}{c_1}\right)\left(\frac{5c_3}{2} + \rho\omega^2\right) + \frac{a_0 b_4}{2}$$
$$\omega_{\theta 6}^p = \left(a_1 + \frac{a_0}{c_1}\right)\left(\frac{13c_7}{2}\right) + \left(\frac{a_0 b_2}{c_1}\right)\left(\frac{9c_5}{2}\right) + \left(\frac{a_0 b_4}{c_1}\right)\left(\frac{5c_3}{2} + \rho\omega^2\right) + \frac{a_0 b_6}{2} \tag{A11}$$

Substituting Eqs. (A10) and (A2) into Eq. (A1) and combining the terms with the same power of r, results in the following equations:

$$\varepsilon_{\theta 0}^p - \varepsilon_{r0}^p = 0,$$
$$8c_3 + (3+v)\rho\omega^2 + E(3\varepsilon_{\theta 2}^p - \varepsilon_{r2}^p) = 0,$$
$$24c_5 + E(5\varepsilon_{\theta 4}^p - \varepsilon_{r4}^p) = 0,$$
$$48c_7 + E(7\varepsilon_{\theta 6}^p - \varepsilon_{r6}^p) = 0, \tag{A12}$$

The substitution of Eq. (A11) into (A12) gives the values of c_3, c_5, and c_7 coefficients in terms of c_1 (not presented here for the sake of brevity).

Fully Plastic Solid Disk. For the case of a fully plastic rotating disk, the boundary condition of the problem is $\sigma_r = 0$ at $r = R$. By substituting the values c_3, c_5, and c_7 in terms of c_1 into Eq. (A3) and satisfying the boundary conditions for c_1, the stresses inside the rotating disk can be obtained according to Eqs. (A3).

Elasto-Plastic Solid Disk. For the case of an elastic plastic rotating disk, let us assume that ς is the radius of plastic region of the disk. Then, stresses in outer elastic region of the disk can be obtained according to ς by solving the governing equations for an elastic rotating hollow disk considering the proper boundary conditions

$$\sigma_r^e = Ar^{-2} + B - \frac{3+v}{8}\rho\omega^2 r^2,$$
$$\sigma_r^e = -Ar^{-2} + B - \frac{1+3v}{8}\rho\omega^2 r^2, \tag{A13}$$
$$\sigma_r^e = 0 \quad \text{at} \quad r = R,$$
$$\sigma_{\text{eq}}^e = \sigma_{\text{yield}} \quad \text{and} \quad \sigma_\theta,\ \sigma_r > 0 \quad \text{at} \quad r = \varsigma \tag{A14}$$

For the inner plastic disk, there are only two unknown constants c_1 and ς, which can be determined by solving the proper boundary conditions

$$\sigma_r^p = \sigma_r^e \quad \text{at} \quad r = \varsigma,$$
$$\sigma_\theta^p = \sigma_\theta^e \quad \text{at} \quad r = \varsigma, \tag{A15}$$

Finally, stresses inside the plastic and elastic regions can be obtained following Eqs. (A3) and (A13), respectively.

Using the proposed analytical method which is discussed briefly above, we re-evaluated the *case*1 problem in Ref. [1] and obtained closer stresses to finite elements results compared to those obtained by You and Zhang. For example, the stress at the center of the disk with the given linear hardening parameters (Eq. (27) in Ref. [1]) was obtained to be equal to 300.8 MPa by our analysis with 0.9% error from the finite element result (298 MPa), compared to the value of ~335 MPa obtained by You and Zhang which has an error equal to ~12.5% compared to the finite element analysis. The error in calculating the elastic–plastic stresses associated with the assumption of linearly hardening material is also reported in Ref. [3], which is erroneous according to our analysis and could be developed as a result of employed solution method.

References

[1] You, L. H., and Zhang, J. J., 1999, "Elastic-Plastic Stresses in a Rotating Solid Disk," Int. J. Mech. Sci., **41**, pp. 269–282.
[2] Güven, U., 1992, "Elastic-Plastic Stresses in a Rotating Annular Disk of Variable Thickness and Variable Density," Int. J. Mech. Sci., **34**, pp. 133–138.
[3] You, L. H., Tang, Y. Y., Zhang, J. J., and Zheng, C. Y., 2000, "Numerical Analysis of Elastic-Plastic Rotating Disks With Arbitrary Variable Thickness and Density," Int. J. Solids Struct., **37**, pp. 7809–7820.
[4] Gamer, U., 1984, "Elastic-Plastic Deformation of the Rotating Solid Disk," Arch. Appl. Mech., **54**, pp. 345–354.
[5] Jahed, H., and Sherkati, S., 2000, "Thermoplastic Analysis of Inhomogeneous Rotating Disk With Variable Thickness," *International Conference Fatigue 2000: Fatigue & Durability Assessment of Materials, Components and*

Structures, M. R. Bache, P. A. Blackmore, J. Draper, J. H. Edwards, P. Roberts, and J. R. Yates, eds., Cambridge, United Kingdom, pp. 229–238.
[6] Eraslan, A. N., and Orcan, Y., 2002, "Elastic-Plastic Deformation of a Rotating Solid Disk of Exponentially Varying Thickness," Mech. Mater., **34**, pp. 423–432.
[7] Eraslan, A. N., and Orcan, Y., 2002, "On the Rotating Elastic-Plastic Solid Disks of Variable Thickness Having Concave Profiles," Int. J. Mech. Sci., **44**, pp. 1445–1466.
[8] Arslan, M. A., 2008, "Flywheel Geometry Design for Improved Energy Storage Using Finite Element Analysis," Mater. Des., **29**, pp. 514–518.
[9] Bhavikatti, S. S., and Ramakrishnan, C. V., 1980, "Optimum Shape Design of Rotating Disks," Comput. Struct., **11**, pp. 397–401.
[10] Chern, J. M., and Prager, W., 1970, "Optimal Design of Rotating Disk for Given Radial Displacement of Edge," J. Optim. Theory Appl., **6**, pp. 161–170.
[11] Danfelt, E. L., Hewes, S. A., and Chou, T.-W., 1977, "Optimization of Composite Flywheel Design," Int. J. Mech. Sci., **19**, pp. 69–78.
[12] Eby, D., Averill, R., Gelfand, B., Punch, W., Mathews, O., and Goodman, E., 1997, "An Injection Island GA for Flywheel Design Optimization," *5th European Congress on Intelligent Techniques and Soft Computing EUFIT '97*, A. Verlag Mainz, ed., Morgan Kaufmann, Aachen, Germany, pp. 687–691.
[13] Krack, M., Secanell, M., and Mertiny, P., 2010, "Cost Optimization of Hybrid Composite Flywheel Rotors for Energy Storage," Struct. Multidiscip. Optim., **41**, pp. 779–795.
[14] Huang, J., and Fadel, G. M., 2000, "Heterogeneous Flywheel Modeling and Optimization," Mater. Des., **21**, pp. 111–125.
[15] Stump, F. V., Paulino, G. H., and Silva, C. N., 2005, "Material Distribution Design of Functionally Graded Rotating Disks With Stress Constraint," 6th World Congresses of Structural and Multidisciplinary Optimization, Rio de Janeiro, Brazil.
[16] Stump, F. V., Silva, E. C. N., and Paulino, G. H., 2007, "Optimization of Material Distribution in Functionally Graded Structures With Stress Constraints," Commun. Numer. Methods Eng., **23**, pp. 535–551.
[17] Funabashi, M., 1997, "Gradient Composites of Nickel Coated Carbon Fibre Filled Epoxy Resin Moulded Under Centrifugal Force," Composites, Part A, **28**, pp. 731–737.
[18] Hashmi, S., and Dwivedi, U., 2007, "Estimation of Concentration of Particles in Polymerizing Fluid During Centrifugal Casting of Functionally Graded Polymer Composites," J. Polym. Res., **14**, pp. 75–81.
[19] Watanabe, Y., Eryu, H., and Matsuura, K., 2001, "Evaluation of Three-Dimensional Orientation of Al3Ti Platelet in Al-Based Functionally Graded Materials Fabricated by a Centrifugal Casting Technique," Acta Mater., **49**, pp. 775–783.
[20] Xie, Y., Liu, C., Zhai, Y., Wang, K., and Ling, X., 2009, "Centrifugal Casting Processes of Manufacturing In Situ Functionally Gradient Composite Materials of Al-19Si-5Mg Alloy," Rare Met., **28**, pp. 405–411.
[21] Bayat, M., Sahari, B. B., Saleem, M., Ali, A., and Wong, S. V., 2009, "Bending Analysis of a Functionally Graded Rotating Disk Based on the First Order Shear Deformation Theory," Appl. Math. Model., **33**, pp. 4215–4230.
[22] Fazelzadeh, S. A., Malekzadeh, P., Zahedinejad, P., and Hosseini, M., 2007, "Vibration Analysis of Functionally Graded Thin-Walled Rotating Blades Under High Temperature Supersonic Flow Using the Differential Quadrature Method," J. Sound Vib., **306**, pp. 333–348.
[23] Güven, U., çelik, A., and Baykara, C., 2004, "On Transverse Vibrations of Functionally Graded Polar Orthotropic Rotating Solid Disk With Variable Thickness and Constant Radial Stress," J. Reinf. Plast. Compos., **23**, pp. 1279–1284.
[24] Librescu, L., Oh, S.-Y., and Song, O., 2005, "Thin-Walled Beams Made of Functionally Graded Materials and Operating in a High Temperature Environment: Vibration and Stability," J. Therm. Stresses, **28**, pp. 649–712.
[25] Librescu, L., Oh, S.-Y., and Song, O., 2004, "Spinning Thin-Walled Beams Made of Functionally Graded Materials: Modeling, Vibration and Instability," Eur. J. Mech. A/Solids, **23**, pp. 499–515.
[26] Oh, S.-Y., Librescu, L., and Song, O., 2005, "Vibration and Instability of Functionally Graded Circular Cylindrical Spinning Thin-Walled Beams," J. Sound Vib., **285**, pp. 1071–1091.
[27] Eraslan, A., and Akis, T., 2006, "On the Plane Strain and Plane Stress Solutions of Functionally Graded Rotating Solid Shaft and Solid Disk Problems," Acta Mech., **181**, pp. 43–63.
[28] Bayat, M., Saleem, M., Sahari, B. B., Hamouda, A. M. S., and Mahdi, E., 2008, "Analysis of Functionally Graded Rotating Disks With Variable Thickness," Mech. Res. Commun., **35**, pp. 283–309.
[29] Durodola, J. F., and Attia, O., 2000, "Deformation and Stresses in Functionally Graded Rotating Disks," Compos. Sci. Technol., **60**, pp. 987–995.
[30] Horgan, C. O., and Chan, A. M., 1999, "The Stress Response of Functionally Graded Isotropic Linearly Elastic Rotating Disks," J. Elast., **55**, pp. 219–230.
[31] Kordkheili, S. A. H., and Naghdabadi, R., 2007, "Thermoelastic Analysis of a Functionally Graded Rotating Disk," Compos. Struct., **79**, pp. 508–516.
[32] Haghpanah Jahromi, B., Farrahi, G. H., Maleki, M., Nayeb-Hashemi, H., and Vaziri, A., 2009, "Residual Stresses in Autofrettaged Vessel Made of Functionally Graded Material," Eng. Struct., **31**, pp. 2930–2935.
[33] Jahed, H., and Dubey, R. N., 1997, "An Axisymmetric Method of Elastic-Plastic Analysis Capable of Predicting Residual Stress Field," ASME J. Pressure Vessel Technol., **119**, pp. 264–273.
[34] Timoshenko, S. P., and Goodier, J. N., 1970, Theory of Elasticity, 3rd ed., McGraw-Hill, New York.
[35] Budiansky, B., 1965, "On the Elastic Moduli of Some Heterogeneous Materials," J. Mech. Phys. Solids, **13**, pp. 223–227.
[36] Chaboche, J. L., Kanouté, P., and Roos, A., 2005, "On the Capabilities of Mean-Field Approaches for the Description of Plasticity in Metal Matrix Composites," Int. J. Plast., **21**, pp. 1409–1434.
[37] Hill, R., 1965, "A Self-Consistent Mechanics of Composite Materials," J. Mech. Phys. Solids, **13**, pp. 213–222.
[38] Love, B. M., and Batra, R. C., 2006, "Determination of Effective Thermomechanical Parameters of a Mixture of Two Elastothermoviscoplastic Constituents," Int. J. Plast., **22**, pp. 1026–1061.
[39] Mori, T., and Tanaka, K., 1973, "Average Stress in Matrix and Average Elastic Energy of Materials With Misfitting Inclusions," Acta Metall., **21**, pp. 571–574.
[40] Saraev, D., and Schmauder, S., 2003, "Finite Element Modelling of Al/SiCp Metal Matrix Composites With Particles Aligned in Stripes—A 2D-3D Comparison," Int. J. Plast., **19**, pp. 733–747.
[41] Vena, P., Gastaldi, D., and Contro, R., 2008, "Determination of the Effective Elastic-Plastic Response of Metal-Ceramic Composites," Int. J. Plast., **24**, pp. 483–508.
[42] Bao, G., Hutchinson, J. W., and McMeeking, R. M., 1991, "Particle Reinforcement of Ductile Matrices Against Plastic Flow and Creep," Acta Metall. Mater., **39**, pp. 1871–1882.
[43] Branch, N. A., Arakere, N. K., Subhash, G., and Klecka, M. A., 2011, "Determination of Constitutive Response of Plastically Graded Materials," Int. J. Plast., **27**, pp. 728–738.
[44] Grujicic, M., and Zhang, Y., 1998, "Determination of Effective Elastic Properties of Functionally Graded Materials Using Voronoi Cell Finite Element Method," Mater. Sci. Eng. A, **251**, pp. 64–76.
[45] Ju, J., and Chen, T., 1994, "Micromechanics and Effective Moduli of Elastic Composites Containing Randomly Dispersed Ellipsoidal Inhomogeneities," Acta Mech., **103**, pp. 103–121.
[46] Yin, H. M., Paulino, G. H., Buttlar, W. G., and Sun, L. Z., 2007, "Micromechanics-Based Thermoelastic Model for Functionally Graded Particulate Materials With Particle Interactions," J. Mech. Phys. Solids, **55**, pp. 132–160.
[47] Yin, H. M., Sun, L. Z., and Paulino, G. H., 2004, "Micromechanics-Based Elastic Model for Functionally Graded Materials With Particle Interactions," Acta Mater., **52**, pp. 3535–3543.
[48] Yin, H. M., Sun, L. Z., and Paulino, G. H., 2005, "A Multiscale Framework for Elastic Deformation of Functionally Graded Composites," Mater. Sci. Forum, **492–493**, pp. 391–396.
[49] Suresh, S., and Mortensen, A., 1998, *Fundamentals of Functionally Graded Materials*, IOM Communications Ltd., London.
[50] Gu, Y., Nakamura, T., Prchlik, L., Sampath, S., and Wallace, J., 2003, "Micro-Indentation and Inverse Analysis to Characterize Elastic-Plastic Graded Materials," Mater. Sci. Eng. A, **345**, pp. 223–233.